第 XX 卷第 XX 期
XXXX 年XX 月

土木与环境工程学报(中英文)
Journal of Civil and Environmental Engineering

Vol. XX No. XX
XX XXXX

DOI：10.11835/j.issn.2096-6717.2026.036

开放科学(资源服务)标识码OSID:

基于参数化CFD与深度学习模型的地铁站活塞效应无组织通风预测

李松,刘猛,李子桥
(重庆大学 土木工程学院,重庆 400045)

摘　要：隧道活塞效应驱动下,穿过站台屏蔽门的无组织通风气流(UVA)对地铁站冷热负荷影响显著,精准的UVA预测是通风空调(HVAC)系统实现节能设计的关键前提。提出一种融合参数化计算流体力学(CFD)与深度学习的智能预测框架,基于不可压缩流体控制方程和k-ε湍流模型,采用ANSYS Fluent开展二维瞬态数值仿真,并将仿真结果作为模型训练数据集。引入新型无量纲参数相对距离比(RDR),用以刻画列车长度与活塞风井间距的耦合效应;仿真工况覆盖不同阻塞比、RDR及4种活塞风井运行状态,且仿真结果经现场实测验证(均方根误差RMSE为0.062 m/s,平均绝对百分比误差MAPE为34.8%,决定系数R^2=0.939)。在此基础上,构建条件编解码模型,实现由静态设计参数对UVA风速完整时间序列的预测。该模型展现出优异的泛化性能,对4个未参与训练的工况均实现高精度预测(R^2>0.94、MAPE<22%),并能有效捕捉列车运行过程中的瞬态风速峰值。

关键词：地铁站;无组织通风气流;活塞效应;CFD仿真;深度学习;编解码模型
中图分类号：TU96　　**文献标志码：**A　　**文章编号：**2096-6717(XXXX)XX-0001-14

Prediction of unorganized ventilation induced by piston effect in subway stations based on parametric CFD and deep learning model

LI Song, LIU Meng, LI Ziqiao
(School of Civil Engineering, Chongqing University, Chongqing 400045, P. R. China)

Abstract: Driven by the tunnel piston effect, unorganized ventilation airflow (UVA) through platform screen doors exerts a considerable influence on subway station cooling and heating loads. Thus, accurate UVA prediction is indispensable to energy-efficient HVAC system design. This study presents an intelligent prediction framework fusing parametric Computational Fluid Dynamics (CFD) and deep learning. Based on incompressible fluid governing equations and the k-ε turbulence model, 2D transient numerical simulations were conducted via ANSYS Fluent, with the results serving as the model's training dataset. A novel dimensionless parameter, the relative distance ratio (RDR), was introduced to depict the coupling effects of train length and piston shaft distance. Simulation scenarios covered blockage ratios, RDR values, and four piston shaft operational states, and were validated by field measurements (RMSE=0.062 m/s, MAPE=34.8%, R^2=0.939). On this basis, a con-

Received: 2026-02-23
Foundation items: Fundamental Research Funds for the Central Universities (No. 2024CDJYXTD-003); 2024 Chongqing University Graduate Student Research Innovation Project (No. CYB240070)
Author brief: LI Song (2000-), main research interests: ventilation and energy efficiency in public buildings, E-mail: 202316021227t@stu.cqu.edu.cn.
LIU Meng (corresponding author), professor, doctorial supervisor, E-mail: liumeng@cqu.edu.cn.
LI Ziqiao (corresponding author), assistant researcher, E-mail: z.li@cqu.edu.cn.

ditional encoder-decoder model was constructed to predict the full UVA wind speed time series from static design parameters. The model exhibited excellent generalization performance, delivering high-accuracy predictions for four untrained working conditions ($R^2 > 0.94$, MAPE $< 22\%$) and effectively capturing transient wind-speed peaks during train operation. This proposed framework acts as a powerful UVA prediction tool, providing technical support for the energy-saving design and intelligent control of subway ventilation systems.

Keywords: subway station; unorganized ventilation airflow (UVA); piston effect; CFD simulation; deep learning; encoder-decoder model

1 Introduction

1.1 Background

By the end of 2024, 58 major cities on the Chinese mainland operated 361 urban rail transit lines totaling 12,160.77 km, with subways (9,306.09 km) accounting for 76.53% of the total. China's urban rail transit is projected to consume 27.023 billion kWh in 2024, and ventilation and air conditioning (VAC) systems typically contribute over one-third of a subway station's operational energy use[1]. Thus, enhancing VAC energy efficiency is pivotal to the sustainable operation of metro systems[2]. Metro trains generate piston wind via head compression and tail negative pressure in tunnels. Most island-platform stations in China feature non-hermetic platform screen doors (PSDs) that open briefly during passenger flow. The wind-induced pressure difference between the platform and the tunnel causes a non-negligible unorganized ventilation airflow (UVA). This UVA impacts both the station thermal environment and VAC energy consumption. Accurate analysis of UVA's dynamic characteristics is essential for optimizing VAC energy savings and has significant practical value for energy conservation in the urban rail transit industry [3].

1.2 Literature review

Tunnel piston wind and UVA in subway stations substantially affect the energy consumption of ventilation and VAC systems, as well as the stations' thermal environment. Extensive research efforts have been devoted to this topic, yielding incremental advances over time. However, existing studies still lack systematicity in research frameworks, generality in methodological approaches, and practical applicability in engineering scenarios.

Current simulations of tunnel piston wind and UVA are categorized into 1D empirical methods and 3D high-fidelity Computational Fluid Dynamics (CFD) approaches. 1D tools (e.g., STESS, SES) enable efficient macro-flow calculations. Luan et al. [4] used STESS to identify tunnel length and train density as UVA drivers and derived a localized UVA volume formula. Liu et al. [5] established a piston wind model highlighting blockage ratio and a multi-factor ventilation design equation. Li et al. [6] further developed a condition-specific air leakage model via STESS under varying tunnel lengths, train densities, and PSD gaps. Hu et al. [7] validated an SES model to link train arrival parameters with UVA and cooling load. While 1D methods are computationally efficient, their empirical formulas and simplified assumptions fail to capture the complete piston wind-to-UVA physics, leading to engineering deviations. In contrast, 3D CFD enables high-precision modeling of complex flow fields. Zhang et al. [8] validated a Bernoulli-based model and derived a unified ventilation rate formula via grey correlation analysis. He et al. [9] quantified piston wind-induced UVA energy savings in transitional seasons across climate zones and verified a novel environmental control system. Zhang et al. [10] built a full-scale 3D CFD model of gapped PSDs to accurately simulate piston wind-PSDs coupling, capturing pressure distributions and recirculation zones. Despite their accuracy, 3D CFD simulations require several days per operational state, severely limiting the feasibility of systematic parametric analysis. Second, most prior studies focus on fixed structural parameters (e.g., tunnel length, ventilation shaft layout) for specific stations, severely limiting the generalizability of their findings beyond the original scenarios. Field experiments aimed at improving simulation reliability are constrained by operational and logistical factors, resulting in limited data scope and poor generalizability [11]. Wang et al. [12] validated a UVA simulation method via field tests, determining the PSD resistance coefficient (0.11-0.35) and providing a measured basis for parameter optimization. Wang et al. [13] explored the UVA-cooling load correlation, designed a measurement method, and conducted limited tests at a Shanghai metro station to analyze UVA distribution at PSDs and entrances/exits. Yang et al. [14] proposed simplified train-induced airflow velocity measurement methods, validated across typical Chinese underground stations. Khaleghi et al. [15] combined experiments and CFD to study a Tehran Metro station, using a layered train speed approach to investigate unsteady airflow during train passage and arrival. AI has demonstrated great potential in subway nonlinear prediction and optimization, yet its integration with CFD for piston wind-induced UVA simulation remains underexplored. Liu et al. [16] verified the feasibility of rapid unsteady piston wind prediction via machine learning, selecting an optimal model from eight algorithms and conducting feature importance analysis. Yin et al. [17] employed BPNN, CCNN, and SVR to accurately predict chiller energy consumption, supporting pre-optimization of VAC parameters. Nam et al. [18] developed a ventilation optimization system combining deep learning and dynamic programming, achieving 8.68% energy savings while maintaining IAQ. Heo et al. [19] applied DQN in a grey-box virtual environment to optimize IAQ control, cutting ventilation energy consumption by 14.4%. Leung et al. [20] used an MLP model to predict weekly energy consumption curves for new station assessment. Subway UVA research faces three core limitations: first, 1D empirical models lack accuracy, while 3D CFD, despite rich outputs, suffers from low computational efficiency; second, field experiments are constrained by operational and site conditions, leading to insufficient data diversity; third, AI's strong nonlinear prediction capability has rarely been integrated with CFD for UVA prediction.

Piston-effect-induced UVA through PSDs significantly affects the thermal load and energy consumption of metro HVAC systems, and accurate UVA prediction is key to the energy-saving design and intelligent regulation of metro ventilation systems. Among existing studies, 1D models rely on empirical coefficients; 3D CFD simulations are computationally inefficient and cannot perform systematic parametric analyses; and field measurements suffer from limited data diversity due to operational constraints. This study generates high-fidelity data using CFD and develops an AI prediction model, proposing an efficient, engineering-applicable UVA prediction method to support the optimal operation of metro environmental control systems.

2 Methodology

This study focuses on an island-platform metro station with PSDs. It conducts 2D transient CFD simulations in ANSYS Fluent based on the incompressible fluid governing equations and the standard k-ε turbulence model. A dimensionless parameter, the RDR, is proposed to characterize the combined effects of key geometric parameters. A large-scale dataset is established from extensive simulation cases covering diverse operational scenarios, and a conditional encoder-decoder architecture is subsequently applied. Following standard preprocessing of static input parameters, encoding is implemented using fully connected layers with residual connections, and decoding is performed via deconvolutional layers and an LSTM. The model enables prediction of 300-second time-resolved wind-speed sequences from static input parameters.

2.1 Simulation methodology

Metro stations are primarily classified by platform layout into island, side, and hybrid island-side types, with island-platform stations widely adopted in China. Statistical data indicate that such stations account for 68%, 61%, 75%, and 60% of the total in Beijing, Shanghai, Wuhan, and Chongqing, respectively [7]. Platform edge doors (PEDs) include several types, such as PSDs and platform barrier doors (PBDs), with PSDs being the dominant type in major Chinese cities like Beijing, Shanghai, Guangzhou, and Chongqing. Thus, an island platform equipped with PSDs is selected as the research prototype for the simulation and application study in this paper, and its simplified model is shown in Fig. 1.

This study adopted ANSYS Fluent for simulation modeling using the finite volume method [21]. 2D CFD was identified as the optimal approach for this research, as it enables accurate and efficient simula-

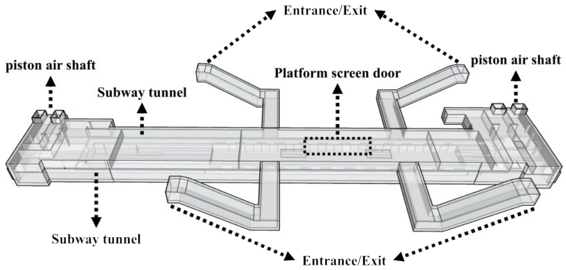

Fig. 1 Island platform underground station with PSDs

tion of the dynamic pressure difference between the tunnel and the platform and provides an effective means for systematic and comprehensive analysis of multi-parameter-coupled flow-field characteristics. Referring to the 3D-to-2D model simplification method proposed by Liu et al. [22], the 3D physical model was converted into the 2D numerical model shown in Fig. 2. The simplification basis for the 2D CFD model is elaborated as follows. Liu et al. validated the accuracy of the 3D CFD model through a 1:20-scale physical experiment and, on this basis, proposed and screened the optimal conversion method for the 2D model, in which the tunnel width is defined as the hydraulic diameter of the 3D cross-section. This method yielded a mean bias error (MBE) of less than 10% for key hydraulic indicators, including piston wind velocity, air volume, and pressure across multiple typical scenarios, such as full-scale tunnels with lengths of 1000 - 5000 m, train operation speeds of 10 - 50 m/s, and subway station-tunnel coupled models. This demonstrates that the 2D model accurately captures the unsteady dynamic characteristics and spatiotemporal distribution patterns of piston wind, providing a well-established academic foundation and methodological reference for developing 2D models in tunnel and subway station ventilation simulation.

Based on the operational characteristics of mainland China's urban rail transit systems, key simulation parameters were defined as follows: the station length was set to 120 m; the tunnel width was adjusted according to the blockage ratio; and the train width was fixed at 3.0 m. The inbound sides of the uplink and downlink tunnels were designated as piston airflow inlets with pressure-outlet boundary conditions, and the platform was also set as a pressure outlet to simulate air exchange with the concourse. The train's inbound side was configured as a velocity inlet, and its outbound side as a pressure outlet. A 0.01 m gap was reserved for closed PSDs to model tunnel-platform air exchange during train arrival and departure. The PSDs opened within 2 s of train arrival (opening width: 2 m), the train dwell time was 30 s, and the PSDs closed 2 s before train departure.

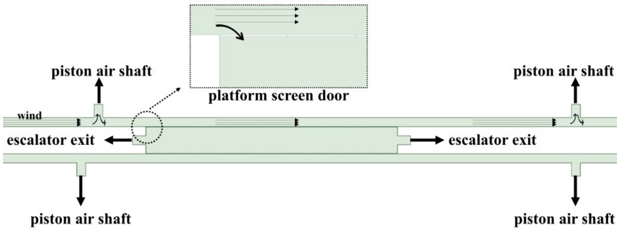

Fig. 2 2D simplified model of a metro station

Given the large number of simulation cases, an unstructured-meshing strategy using triangular elements was adopted. Meshing parameters were normalized across all cases: the maximum mesh size was 0.2 m, the minimum 0.002 m, and the growth rate was 1.13. The number of mesh elements ranged from 150,000 to 200,000, with an average element quality above 0.7 and a skew of approximately 0.15. Topological assessments verified mesh completeness with no anomalies detected. Transient simulations were conducted with a fixed time step of 0.01 s and 20 iterations per step, with a convergence criterion of a residual below 10^{-4}. This study used ANSYS Fluent 2024 R2 to perform transient numerical simulations of metro piston wind effects, employing the fundamental governing equations for incompressible fluids [23].

$$\frac{\partial \rho}{\partial t}+\nabla\cdot(\rho\vec{v})=0 \tag{1}$$

$\frac{\partial \rho}{\partial t}$: the rate of change of fluid mass per unit volume over time; $\nabla\cdot(\rho\vec{v})$: the net mass flux out of a unit volume due to velocity.

$$\frac{\partial(\rho\vec{v})}{\partial t}+\nabla\cdot(\rho\vec{v}\vec{v})=-\nabla p+\nabla\cdot(\mu\nabla\vec{v})+f_v \tag{2}$$

$\frac{\partial(\rho\vec{v})}{\partial t}$: the rate of change in momentum per unit volume of fluid over time; $\nabla\cdot(\rho\vec{v}\vec{v})$: the net momentum flux out of a unit volume owing to the velocity; $-\nabla p$: the pressure force acting on the fluid per unit volume; $\nabla\cdot(\mu\nabla\vec{v})$: the viscous stress acting on the fluid per unit volume; f_v: the body force source term per unit volume of fluid. The standard k-ε

turbulence model was used.

$$\frac{\partial}{\partial t}(\rho k)+\frac{\partial}{\partial x_j}(\rho k u_i)=\frac{\partial}{\partial x_j}\left[\left(\mu+\frac{\mu_t}{\sigma_k}\right)\frac{\partial k}{\partial x_j}\right]+ G_k+G_b-\rho\varepsilon-Y_M \tag{3}$$

$$\frac{\partial}{\partial t}(\rho\varepsilon)+\frac{\partial}{\partial x_i}(\rho\varepsilon u_i)=\frac{\partial}{\partial x_i}\left[\left(\mu+\frac{\mu_t}{\sigma_\varepsilon}\right)\frac{\partial\varepsilon}{\partial x_j}\right]+ C_{1\varepsilon}\frac{\varepsilon}{k}(G_k+C_{3\varepsilon}G_b)C_{2\varepsilon}\rho\frac{\varepsilon^2}{k} \tag{4}$$

$$\mu_t=C_\mu\rho\left(\frac{k^2}{\varepsilon}\right) \tag{5}$$

The model constants are: $C_{1\varepsilon}=1.44$, $C_{2\varepsilon}=1.92$, $C_\mu=0.09$, $\sigma_k=1.00$, $\sigma_\varepsilon=1.30$. A pressure-based solver was employed, with pressure-velocity coupling implemented via the SIMPLE (Semi-Implicit Method for Pressure-Linked Equations) algorithm. Train motion was defined using a user-defined function (UDF), and dynamic meshing was realized through a combined strategy of spring-based smoothing and local remeshing. Convergence was achieved when all residual values fell below 10^{-4} at each time step.

Based on the literature reviewed, the key factors governing piston wind-induced UVA at subway platforms are the blockage ratio, train length, the operational status of the piston wind shafts, and the shaft-to-platform distance. Preliminary analysis indicates that train length and shaft-to-platform distance are geometric parameters with interdependent effects on UVA. Treating them as independent variables leads to two critical limitations: first, conclusions from dimensional parameters are scenario-specific and lack generalizability across stations with different train lengths or shaft layouts; second, their significant interaction effect may be overlooked, resulting in incomplete mechanistic interpretations and potential bias. To address this, a comprehensive dimensionless parameter is proposed to capture their coupling and eliminate dimensional constraints, enabling uniform characterization of train-shaft geometric effects on UVA across diverse scenarios. This study introduces the relative distance ratio ($\mathrm{RDR}=\frac{D_{\text{shaft}}}{L_{\text{train}}}$). This novel dimensionless number condenses the two geometric scales into a single quantity that describes their relative relationship. Its physical meaning clarifies how system geometry influences UVA, avoiding the confounding effects of absolute dimensions and enhancing the generalizability of findings. Training data for the AI model were generated using parametric simulations, with parameters determined from prior studies and relevant metro design specifications in mainland China, as summarized in Table 1.

Table 1　Simulation parameter settings

Blockage Ratio	RDR	Piston Shaft Opening/Closing Status
0.4	0.2	All Open
0.5	0.4	Close Entrance-side Shaft
0.6	0.7	Close Exit-side Shaft
0.7	1.0	All Closed
0.7	1.2	All Closed

2.2　Deep learning prediction model

To mitigate biases in association mining arising from variations in numerical magnitudes, data standardization is essential.

$$x_{\text{norm}}=\frac{x-x_{\min}}{x_{\max}-x_{\min}} \tag{6}$$

x: the original parameter value; $x_{\min}$: the minimum values of the parameter in the CFD dataset; $x_{\max}$: the maximum values of the parameter in the CFD dataset; x_{norm}: the standardized value. The opening/closing status of the ventilation shafts is a discrete parameter, digitized using one-hot encoding [24]. The states of air shafts, including all open, all closed, closing the piston air shaft on the inbound side, and closing the piston air shaft on the outbound side, are named S_1, S_2, S_3 and S_4 respectively. The encoding formula is as follows.

$$S_{\text{one-hot}}=\begin{cases}[1,0,0,0](S=S_1)\\ [0,1,0,0](S=S_2)\\ [0,0,1,0](S=S_3)\\ [0,0,0,1](S=S_4)\end{cases} \tag{7}$$

This encoding method can sufficiently reduce numerical bias in discrete parameters and clearly enforce mutual exclusivity among all states. In addition, the nonlinear effect of shaft status on UVA is improved. The essence of the conditional encoder-decoder architecture is to split the prediction process into two parts: encoding and decoding [25]. The encoding process compresses the input condition x_c into a condition code z_c (Condition Code), which can be expressed as:

$$z_c=E(x_c;\theta_E) \tag{8}$$

θ_E: the learnable parameters of the encoder. This study employs a hybrid approach within the encoder, integrating fully connected layers with residual connections to facilitate the abstraction of essential features from static parameters[26]:

$$h_l = \sigma(W_l h_{l-1} + b_l) + h_{l-1} \tag{9}$$

l: the network layer number of the encoder; h_{l-1}: the input feature vector to the $l-1$ layer; W_l: the weight matrix of the l layer; b_l: the bias vector of the l layer; $\sigma(\cdot)$: the activation function. Decoding takes the aforementioned condition code z_c as input and reconstructs the target dynamic sequence $\hat{y}$, which can be expressed as:

$$\hat{y} = D(z_c;\theta_D) \tag{10}$$

θ_D: the learnable parameters of the decoder. This study employed a hybrid decoder architecture, integrating deconvolutional layers with Long Short-Term Memory (LSTM) networks to enable dynamic sequence generation. The deconvolution process can be represented as follows[27]:

$$h = \mathrm{ConvTranspose1}d(z_c; W, b, k, s, p) \tag{11}$$

W: the deconvolution matrix; b: the deconvolution bias vector; k: the kernel size; s: the kernel stride; p: the zero-padding amount. We used the deconvolution results as the LSTM's initial memory state, enabling the LSTM to generate temporal features through gating mechanisms and dynamic feedback in a stepwise manner. The LSTM network retains selective memory of temporal information through its three gating units and cell state, effectively addressing the vanishing-gradient problem associated with traditional Recurrent Neural Networks (RNNs).

$$\text{Forget gate: } f_t = \sigma(W_f \cdot [h_{t-1}, x_t] + b_f) \tag{12}$$

$$\text{Input gate: } \begin{cases} i_t = \sigma(W_i \cdot [h_{t-1}, x_t] + b_i) \\ \tilde{C}_t = \tanh(W_C \cdot [h_{t-1}, x_t] + b_C) \end{cases} \tag{13}$$

$$\text{Cell state update: } C_t = f_t \odot C_{t-1} + i_t \odot \tilde{C}_t \tag{14}$$

$$\text{Output gate: } \begin{cases} o_t = \sigma(W_o \cdot [h_{t-1}, x_t] + b_o) \\ h_t = o_t \odot \tanh(C_t) \end{cases} \tag{15}$$

In summary, the complete forward propagation process of the model, from input to output, can be expressed as:

$$\hat{y} = D(E(x_c;\theta_E);\theta_D) = F(x_c;\theta) \tag{16}$$

F: the entire conditional encoder-decoder network; $\theta = \{\theta_E, \theta_D\}$: the set of parameters to be optimized. The objective of the model is to learn the optimal parameters θ through training, such that the predicted sequence $\hat{y}$ approximates the true sequence y as closely as possible. The logical framework of the conditional encoder-decoder architecture is depicted in Fig. 3.

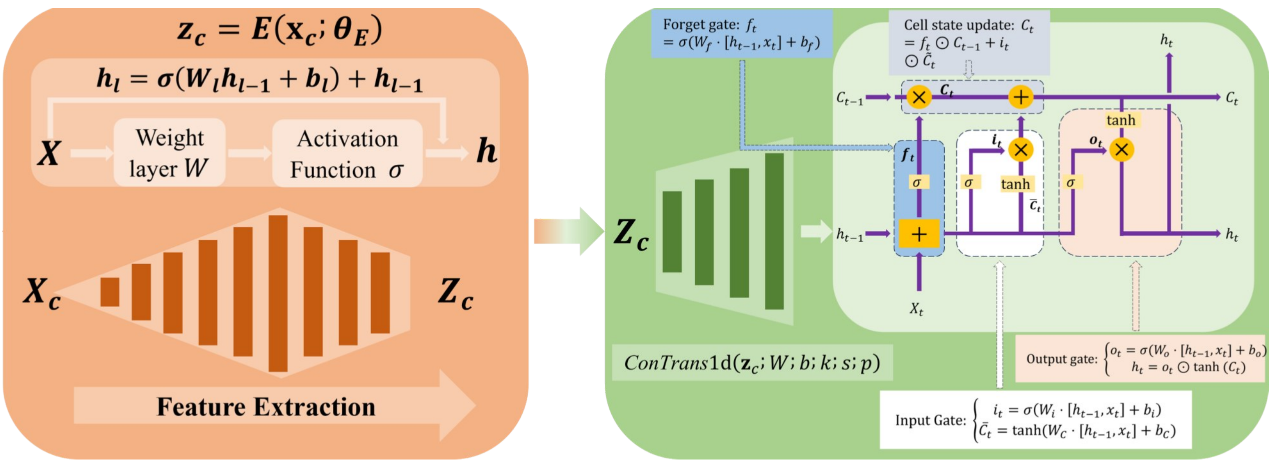

Fig. 3 Principles of the conditional encoder-decoder architecture

2.3 Field Verification Method

This field experimental test is conducted at an island platform station on the Chongqing Metro under standardized night-time conditions with no passenger interference, as shown in Fig. 4. Its primary objective is to validate the accuracy and reliability of the CFD simulation model, rather than serving as the core method for data acquisition in this study. The core UVA wind speed dataset of this research is primarily generated through multi-dimensional, multi-parameter, 2D transient CFD simulations that cover different blockage ratios, RDRs, and various operating states of the piston wind shafts. This approach ensures the dataset's completeness, diversi-

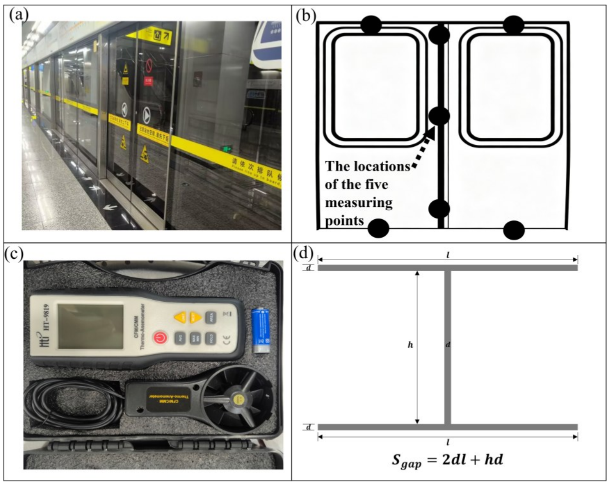

Fig. 4　Field measurement schematic

ty, and comprehensive parameter coverage. The proposed model is specifically designed for island-platform metro stations equipped with PSDs. For a single train entry and exit process, it can achieve time-series prediction of wind speed induced by screen-door penetration across combinations of blockage ratios, RDRs, and on/off states of the piston wind shafts. Other station types, such as side-platform stations and island-side combined stations, as well as train operation strategies, including multi-train continuous operation and peak-hour dense departure schedules, along with external boundary conditions, such as extreme meteorological conditions and different tunnel lining types, are temporarily beyond the scope of this study. Content related to these aspects will be addressed as core future research directions through expanding the range of parameter simulations and supplementing with multi-scene field validations.

3　Results

3.1　Flow field characteristics analysis

In this section, the accuracy of the numerical simulation model is verified by comparing the simulation results with the physical phenomenon of subway piston effect under normal operating conditions (RDR $=0.2$, blockage ratio$=0.7$, all piston wind shafts open) in transient simulations. As shown in Fig. 5, the airflow field distribution at $t=18$ s (train arrival at the station) is presented.

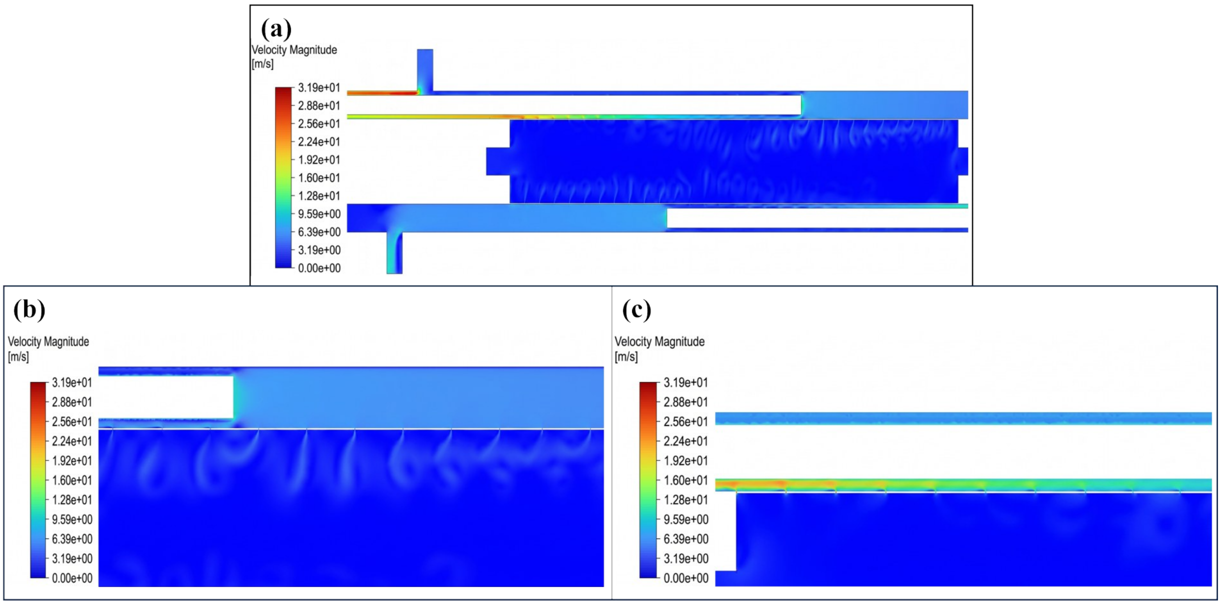

Fig. 5　Airflow field of an arriving train

As shown in Fig. 5(a), upon train arrival at the station, the air ahead of the train is pushed backward. The high axial velocity inside the tunnel indicates that most of this air is propelled forward by the incoming train. Fig. 5(b) reveals significant air displacement at PSD gaps and flow curvature from the gaps to the platform area. Fig. 5(c) illustrates air shear flow along the train sides and tunnel wall, resulting in a fully developed flow field around the train. Fig. 5 presents the airflow field distribution at train departure ($t=68$ s):

Fig. 6(a) illustrates the global reversal of the flow field at the onset of train movement, with airflow directed from the platform and the entrance-side piston shafts into the tunnel. Air from the platform and the piston shaft behind the train fills the void left

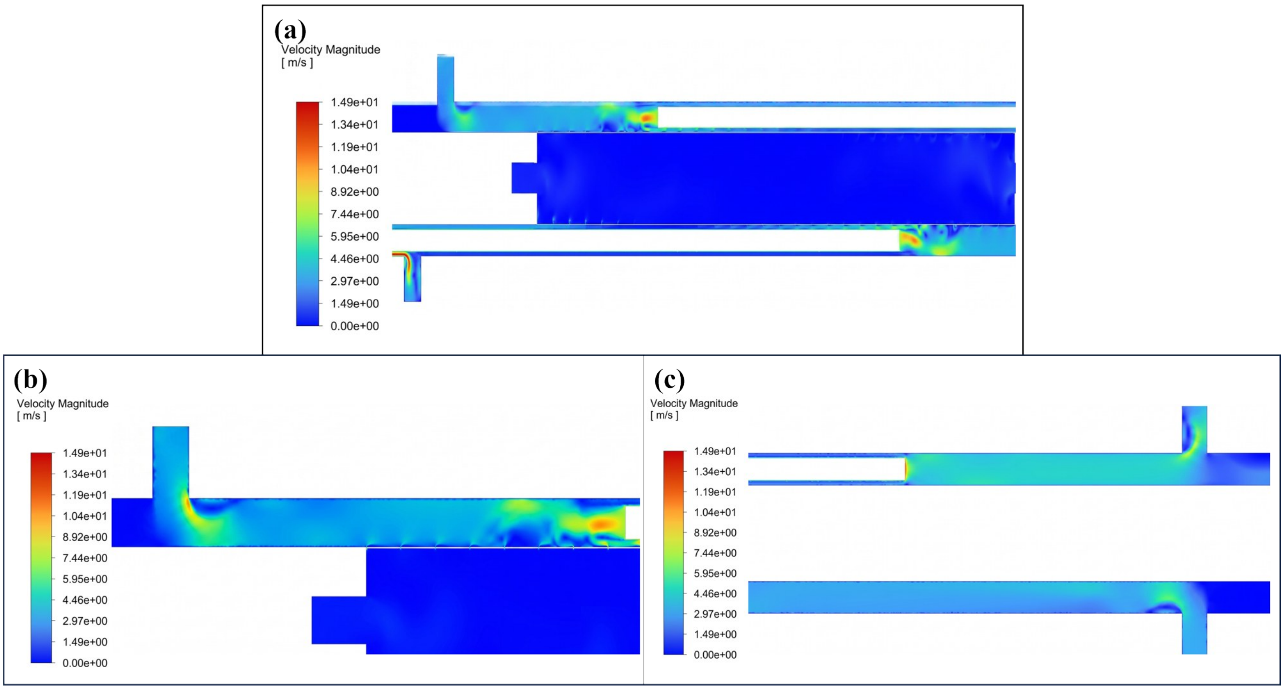

Fig. 6 Airflow field of a departing train

by the departing train, maintaining air pressure balance. Fig. 6(b) shows that the main flow activity concentrates at the train's tail rear, generating high-speed concentrated suction airflow— the primary driving force for departure piston wind— which draws air from the rear piston shaft and platform. Fig. 6(c) indicates that as the train departs the station, airflow velocity behind the train head gradually increases; however, due to the exit-side piston shaft, nearly all piston wind is discharged through it. This section initially explores the effects of key design parameters on subway station UVA volume using the control variable method and the working conditions in Table 1, with the findings presented as follows.

Fig. 7(a) depicts the influence of piston shaft operating modes on UVA under RDR=0.2 and blockage ratio=0.7. Wind speed peaked when all piston shafts were closed, indicating improper release of the piston wind effect; conversely, wind speed was minimal and varied smoothly when all shafts were fully open, demonstrating their effectiveness in reducing pressure and guiding air. Closing either the entrance-side or exit-side piston shaft enhanced positive pressure during train arrival and negative pressure during departure, causing wind speed fluctuations relative to fully open/closed states, but not to a full extent. Fig. 7(b) illustrates RDR's effect on UVA at blockage ratio=0.7 (all piston shafts open). Lower RDR (closer piston shafts to the platform or longer trains) reduced UVA airflow rate; in contrast, RDR=1.0 - 1.2 (farther piston shafts or shorter trains) increased UVA airflow, weakened the effectiveness of shaft regulation, and elevated airflow through PSDs. Fig. 7(c) examines the blockage ratio's impact on UVA (all piston shafts open, RDR=0.2). Increasing blockage ratio significantly amplified UVA wind speed variation, with more pronounced fluctuations at 0.4 - 0.7. Higher blockage ratios intensify the train piston effect, boosting tunnel airflow vigor and increasing PSD-transmitted unorganized ventilation.

To enhance the engineering applicability and reliability of the research conclusions, this study conducts a comparative analysis of extreme operating conditions based on the original core working conditions(blockage ratio, RDR, and piston wind shaft status). It focuses on the UVA response laws under extreme parameter combinations, such as a high blockage ratio (BR=0.7) and an extreme RDR (1.2). Analysis of Fig. 7(b) reveals that the peak UVA wind speed during the exit phase exhibits a significant cumulative effect with the increase of the RDR value. Under the extreme working condition of RDR=1.2, the fluctuation amplitude of wind speed during the exit phase is significantly higher than that under other conventional working conditions (RDR=0.2~

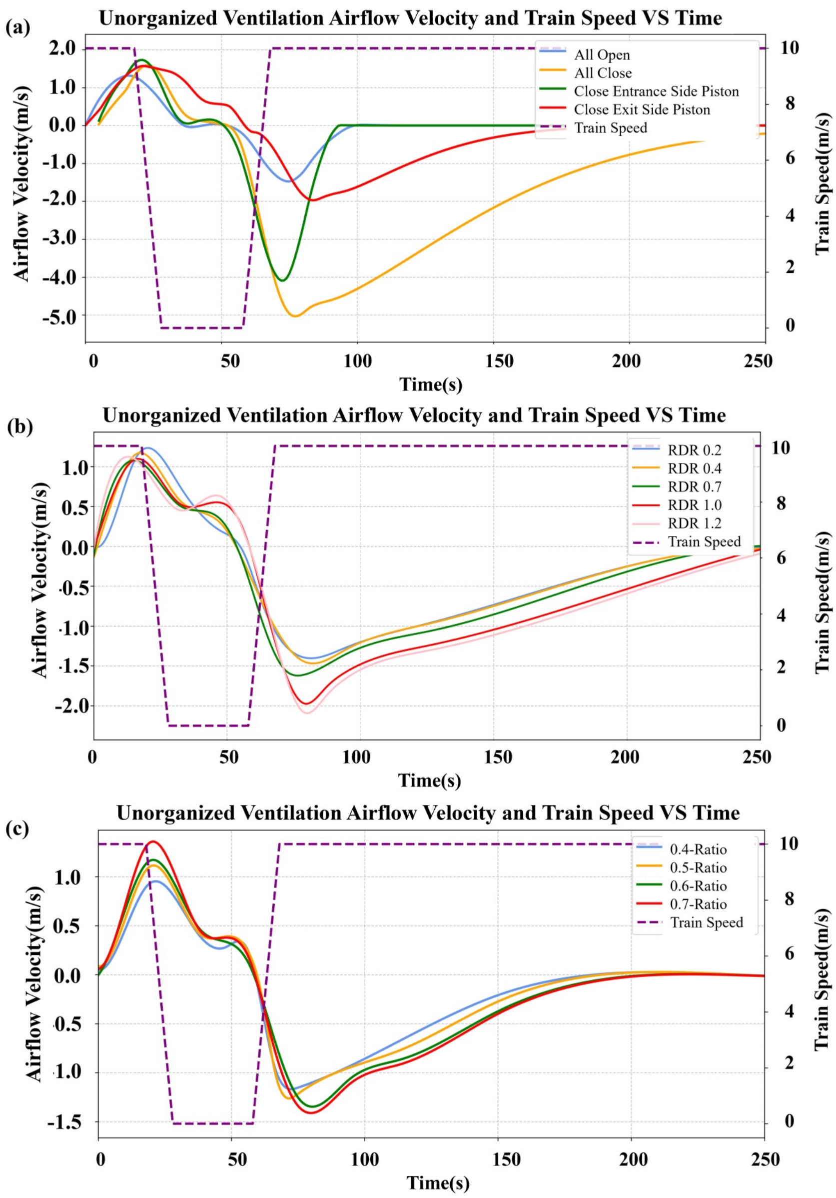

Fig. 7　Airflow velocity under different opening/closing conditions of piston wind shafts

0.7). This physical law indicates that when the piston wind shafts are arranged close to the platform or long-marshaling trains are adopted, the high-pressure airflow generated by the piston wind cannot diffuse over long tunnel distances and instead directly acts on the gaps of the PSDs, resulting in peak UVA intensity. Fig. 7(c) shows the flow field characteristics under the extreme working condition of a high blockage ratio. The results demonstrate that as the blockage ratio increases from 0.4 to 0.7, the peak UVA wind speed during the entrance phase (train arrival phase) rises accordingly, and the peak wind speed during the exit phase is also significantly higher than under other working conditions. Physically, a high blockage ratio indicates a large difference between the cross-sectional area of the train and that of the tunnel, leading the train to reach a critical state with respect to air-pushing and suction efficiency.

3.2　Field measurements and model validation results

Fig. 8 compares the temporal evolution of measured and CFD-simulated UVA wind speeds at the corresponding position and direction under the above conditions. The CFD-simulated wind speed curve showed good consistency with the measured data, effectively capturing the two main wind speed peaks and their variations during train arrival and departure. Furthermore, RMSE, MAPE, and R^2 were used to evaluate simulation accuracy: RMSE reflects the absolute error between simulated and measured data, MAPE indicates the relative error of simulated results, and R^2 denotes the model's ability to explain the variation in measured data.

$$E_{\mathrm{RMSE}}=\sqrt{\frac{1}{n}\sum_{i=1}^{n}\left(y_i-\widehat{y_i}\right)^2} \tag{17}$$

$$E_{\mathrm{MAPE}}=\frac{100\%}{n}\sum_{i=1}^{n}\left|\frac{y_i-\hat{y}_i}{y_i}\right| \tag{18}$$

$$R^2=1-\frac{\sum_{i=1}^{n}\left(y_i-\widehat{y_i}\right)^2}{\sum_{i=1}^{n}\left(y_i-\overline{y_i}\right)^2} \tag{19}$$

E_{RMSE}: value of RMSE calculation result; E_{MAPE}: value of MAPE calculation result; n: total number of data points; y_i: the i -th measured value; $\hat{y}_i$: the i -th simulated value; $\bar{y}=\frac{1}{n}\sum_{i=1}^{n}y_i$: the mean of the measured values.

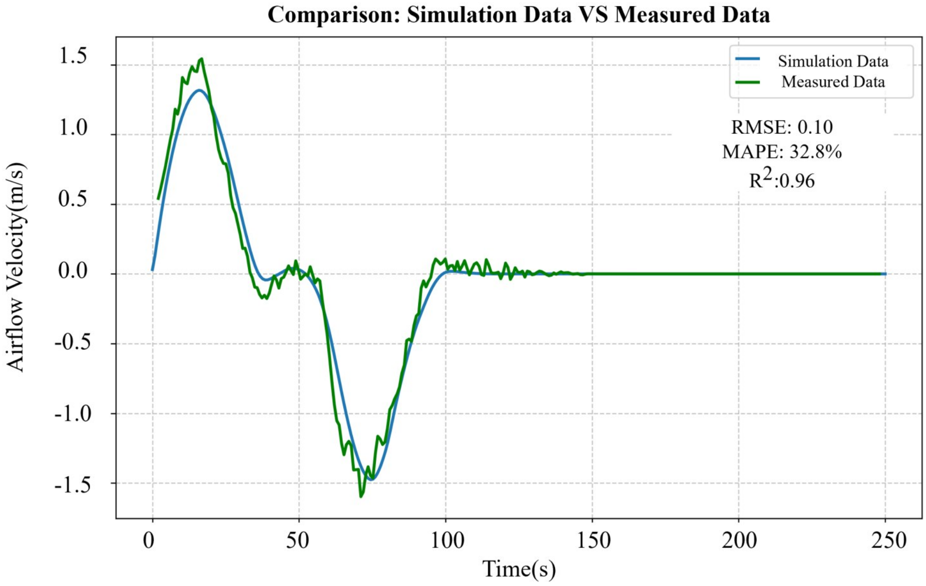

Fig. 8 Comparison between measured and CFD simulation results

The RMSE, MAPE, and R^2 values for field results compared with CFD simulations for unorganized ventilation wind speed are calculated as follows: RMSE = 0.062 m/s, MAPE = 34.8%, and R^2 = 0.939. There is a strong correlation between the CFD model results and the empirical survey, indicating high model reliability.

3.3 Wind speed prediction results using conditional encoder-decoder

Four operating conditions other than the training set were randomly chosen as validation cases: Prediction Case A: Blockage ratio = 0.4, RDR = 0.4, and all piston shafts closed; Prediction Case B: Blockage ratio = 0.5, RDR = 0.7, and entrance-side piston shaft closed; Prediction Case C: Blockage ratio = 0.6, RDR = 1.0, and exit-side piston shaft closed; Prediction Case D: Blockage ratio = 0.6, RDR = 1.2, and all piston shafts closed. The prediction results are illustrated in Fig. 9.

Specifically, the conditional encoder-decoder model's prediction metrics for wind speed data are as follows: Case A: RMSE = 0.105 m/s, MAPE = 15.3%, R^2 = 0.978; Case B: RMSE = 0.097 m/s, MAPE = 18.2%, R^2 = 0.951; Case C: RMSE = 0.113 m/s, MAPE = 22%, R^2 = 0.947; Case D: RMSE = 0.109 m/s, MAPE = 19.8%, R^2 = 0.953. All error ranges are acceptable, strongly verifying the model's excellent prediction performance for UVA wind speed under diverse operational conditions.

This study employs data generated through CFD simulations for model training, rather than directly utilizing field measurement data. This approach lies in the significant limitations associated with acquiring field measurement data from engineering projects. On the one hand, conducting on-site tests at metro stations requires approval from the operating authorities. Train operations and passenger flows constrain test duration, and numerous interfering factors make it challenging to conduct full-scope tests across multiple parameters and operating conditions. On the other hand, obtaining field measurement data that matches the parameters of this study would require on-site testing at more than ten metro

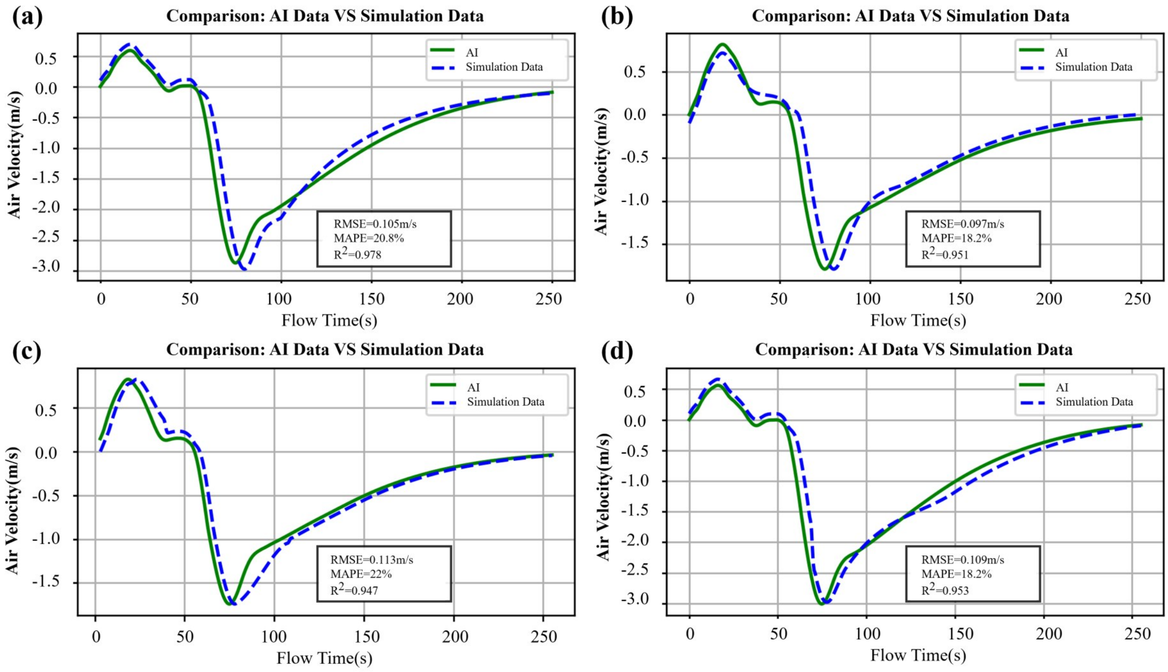

Fig. 9　Conditional encoder-decoder airflow velocity prediction results

stations with distinct structural parameters, resulting in substantial time and resource consumption and extremely low data acquisition efficiency.

3.3　UVA load calculation

UVA load is a key dynamic component of the air-conditioning cooling load in the public areas of subway stations with PSD systems. Driven by the piston effect in train tunnels, hot, humid air on the tunnel side infiltrates the platform side through PSD gaps, forming this load. The load magnitude is correlated with the UVA air volume and the enthalpy difference of the air between the tunnel and platform sides. It is also affected by station design parameters. Based on the conditional encoder-decoder model for predicting the time series of PSD leakage air volume and the calculation method for PSD leakage air load constructed above, an accurate hourly prediction of PSD leakage air load can be realized.

An hourly cooling load prediction model for PSD leakage air was established using the enthalpy difference method and the predicted time series of UVA air volume. It is divided into three dimensions: total cooling load, sensible heat load, and latent heat load. The calculation formula for the hourly total cooling load of leakage air is as follows:

$$Q_{\mathrm{psd}}(t)=\rho \cdot Q_p(t) \cdot (i_t(t)-i_s)\times 1000$$

where $Q_{\mathrm{psd}}(t)$ is the hourly total cooling load of PSD leakage air in the t-th time period; $Q_p(t)$ is the hourly PSD UVA air volume in the t-th time period, converted from the hourly transient UVA wind speed predicted by the aforementioned conditional encoder-decoder model; $i_t(t)$ is the air enthalpy on the tunnel side in the t-th time period, which can be calculated from the hourly temperature and humidity on the tunnel side according to the psychrometric equation of moist air; i_s is the design air enthalpy in the platform public area. The conversion formula for the hourly UVA air volume is:

$$Q_p(t)=v(t) \cdot S_{\mathrm{gap}}$$

where $v(t)$ is the hourly transient average wind speed at the PSD gap in the t-th time period, predicted by the conditional encoder-decoder model; S_{gap} is the total gap area of PSDs, and the calculation formula for the single PSD gap area is:

$$S_{\mathrm{gap,single}}=2dl+hd$$

where d is the width of the PSD gap; l is the horizontal length of the PSD; h is the vertical height of the PSD. The calculation formulas for the hourly sensible heat load and latent heat load of leakage air are as follows:

$$Q_{\mathrm{psd},s}(t)=\rho \cdot c_p \cdot Q_p(t) \cdot (t_t(t)-t_s)\times 1000$$

$$Q_{\mathrm{psd},l}(t)=Q_{\mathrm{psd}}(t)-Q_{\mathrm{psd},s}(t)$$

where $Q_{\mathrm{psd},s}(t)$ is the hourly sensible heat load of PSD leakage air in the t-th time period; $Q_{\mathrm{psd},l}(t)$ is the hourly latent heat load of PSD leakage air in the t-th time period; c_p is the constant pressure specific heat capacity of air; $t_t(t)$ is the dry-bulb temperature on the tunnel side in the t-th time period; t_s is the design dry-bulb temperature in the platform public area.

The conditional encoder-decoder model for PSD leakage air volume prediction constructed above takes the blockage ratio, RDR, and piston shaft operating status as the core input parameters, and outputs the time series curve $v(t)$ of the UVA wind speed for the full cycle of train arrival and departure. Substituting the hourly wind speed $v(t)$ output by the model directly into the calculation formulas yields the hourly UVA air volume $Q_p(t)$. Using the enthalpy difference, air density, and other parameters determined in accordance with relevant codes, the hourly prediction of leakage air load can be achieved, thereby establishing an end-to-end connection from parameter prediction to air volume conversion and, ultimately, to load calculation.

The high prediction accuracy of the UVA model in this study is a fundamental guarantee for the precise calculation of PSD leakage air load. It is crucial for cooling/heating load calculation, air supply control, and energy optimization of subway stations. Under untrained conditions, the model still achieves high-precision wind speed prediction with R-squared > 0.94 and MAPE $< 22\%$, thereby controlling leakage air load calculation errors, avoiding excessive overall load deviation, and reducing energy waste. It can also accurately predict UVA wind-speed time series and load changes in advance, providing reliable feedforward control for air-supply systems and reducing the energy consumption of fans and water pumps. Furthermore, the model enables high-precision hourly prediction of leakage air load, supporting refined, demand-based operation of HVAC systems, reducing mechanical ventilation energy consumption during transitional seasons, and minimizing the inefficient energy consumption of equipment such as chillers in summer and winter, thereby demonstrating its practical engineering value.

4 Discussion

This study adopted an integrated approach combining 2D parametric CFD simulations with a conditional encoder-decoder model to predict piston-effect-driven UVA in metro stations accurately. Based on the incompressible fluid governing equations and the k-ε turbulence model, 2D transient simulations were carried out. A dimensionless parameter, the RDR, was defined to characterize the coupling effect of train length and piston wind shaft spacing, and the impacts of piston wind shaft operational states, blockage ratios, and RDR on the UVA flow field were systematically analyzed.

Field measurements at a station on the Chongqing Metro verified the proposed method's validity, with the CFD simulation results showing a high degree of agreement with the measured data (RMSE $= 0.062$ m/s, MAPE $= 34.8\%$, $R^2 = 0.939$), thereby providing a high-fidelity dataset for model training. The conditional encoder-decoder model exhibited excellent generalization performance across four untrained working conditions ($R^2 > 0.94$, MAPE $< 22\%$). It could accurately capture transient wind-speed peaks during train arrivals and departures, enable direct mapping from static design parameters to dynamic UVA wind-speed time series, and achieve prediction efficiency far superior to that of 2D CFD simulations, thus meeting the demand for rapid multi-scenario evaluation in engineering practice.

This study has certain limitations. Firstly, the range of simulated parameters is limited, resulting in insufficient generalization ability of the model under extreme working conditions. Secondly, the simplified 2D CFD processing fails to accurately characterize the 3D flow field in local areas of the station, such as entrances, exits, and escalators. Thirdly, meteorological parameters such as temperature and humidity are not incorporated. In addition, the research object is limited to island-platform metro stations equipped with fully enclosed PSDs, and the study is conducted only under single-train arrival and departure conditions, without covering side-platform/island-side hybrid stations or multi-train continuous operation scenarios.

Future research will conduct targeted optimizations to expand the scope of parametric simulation to construct a larger-scale training dataset; adopt a hybrid method of 2D and 3D CFD to balance computational efficiency and simulation accuracy; integrate meteorological parameters and real-time metro operation data, extend the research scenarios to different station types and multi-train operation conditions, and develop a multi-feature prediction model to improve the engineering applicability of the model in the intelligent control of ventilation systems.

5 Conclusion

For island-platform metro stations equipped with PSDs, this study established a data-driven prediction model for piston-effect-driven UVA. Additionally, it developed a technical route comprising parametric CFD simulation, deep learning modeling, and dynamic UVA prediction, which provides specific technical support for the energy-saving design and practical regulation of metro VAC systems.

By conducting 2D transient CFD simulations that considered the blockage ratio, RDR, and piston wind shaft operational states, a high-quality UVA dataset was constructed. The designed conditional encoder-decoder network realizes the direct mapping from static parameters to UVA wind speed time series, and field measurements and untrained working conditions have fully verified its effectiveness. The proposed dimensionless RDR eliminates limitations arising from absolute dimensions and enables unified characterization of UVA laws across different station geometries. Meanwhile, the influence laws of core parameters are clarified: increases in blockage ratio and RDR both intensify UVA intensity, and the two parameters exhibit strong nonlinear coupling with UVA; fully opening the piston wind shafts is a key measure to suppress fluctuations in UVA wind speed and regulate platform pressure.

The integrated framework of CFD and deep learning developed in this study addresses the dilemma that traditional UVA prediction methods struggle to balance accuracy and efficiency. The 2D CFD model, verified by field measurements($R^2=0.939$), serves as an efficient tool for generating training data. Notably, the conditional encoder-decoder model achieves a high prediction accuracy of $R^2>0.94$ under untrained working conditions. This greatly shortens computation time compared with traditional CFD methods and enables the transformation of UVA prediction from case-based simulation to real-time computation, making it directly applicable to rapid, multi-scenario UVA evaluation in the preliminary stage of engineering projects.

Future research will focus on improving the generalization ability of the model by expanding the parametric simulation space to incorporate extreme working conditions and local structural parameters; combining with 3D CFD simulation for verification and supplementation to optimize dataset generation; integrating meteorological and operational data, extending the research scope to side-platform/island-side hybrid stations and multi-train operation conditions, and developing a multi-scenario prediction model to adapt to the demand for refined practical management and control of metro ventilation systems.

References

[1] Feng Z B, Chen W Y, Liu Y, et al. Long-term equilibrium relationship analysis and energy-saving measures of metro energy consumption and its influencing factors based on cointegration theory and an ARDL model[J]. Energy, 2023, 263: 125965.

[2] Casals M, Gangolells M, Forcada N, et al. A breakdown of energy consumption in an underground station [J]. Energy and Buildings, 2014, 78: 89-97.

[3] Zhang Y, Li X F. A study of fresh air control in subway stations[J]. Journal of Wind Engineering and Industrial Aerodynamics, 2018, 175: 384-390.

[4] Luan C Z, Li X F. Piston wind in subway stations with platform bailout doors: dynamics and calculation[J]. Energy and Buildings, 2025, 346: 116206.

[5] Liu M Z, Zhang H, Zhu C G, et al. Theoretical modeling of piston wind induced by multiple trains in longitudinal tunnel[J]. Sustainable Cities and Society, 2020, 57: 102127.

[6] Li X F, Wang Y. Simulation study on air leakage of platform screen doors in subway stations[J]. Sustainable Cities and Society, 2018, 43: 350-356.

[7] Hu M Q, Liu M, You D, et al. Influence of train arrival characteristics on unorganized ventilation in underground subway station with platform screen doors[J]. Journal of Wind Engineering and Industrial Aerodynamics, 2020, 198: 104089.

[8] Zhang H, Zhu C G, Liu M Z, et al. Mathematical modeling and sensitive analysis of the train-induced unsteady airflow in subway tunnel[J]. Journal of Wind Engineering and Industrial Aerodynamics, 2017, 171: 67-78.

[9] He D Q, Teng X L, Chen Y J, et al. Piston wind characteristic and energy saving of metro station environmental control system[J]. Journal of Building Engineering,

2021, 44: 102664.

[10] Zhang J, Wang J Y, Yang Q S, et al. Simulation of piston effects on platform screen doors considering air leakage[J]. Atmosphere, 2022, 13(12): 1967.

[11] He D Q, Teng X L, Chen Y J, et al. Energy saving in metro ventilation system based on multi-factor analysis and air characteristics of piston vent[J]. Applied Energy, 2022, 307: 118295.

[12] Wang Y, Li X F. Unorganized ventilation in subway stations with Platform Screen Doors[J]. Building and Environment, 2017, 125: 556-564.

[13] Wang J W, Yin Y S, Wei Z Q, et al. Experimental investigation on cooling load caused by unorganized ventilation in subway station: a case study[J]. Energy and Buildings, 2024, 320: 114574.

[14] Yang L, Zhang Y C, Xia J J. Case study of train-induced airflow inside underground subway stations with simplified field test methods[J]. Sustainable Cities and Society, 2018, 37: 275-287.

[15] Khaleghi M, Talaee M R. Analysis of unsteady airflow in a subway station influenced by train movement[J]. Science and Technology for the Built Environment, 2020, 26(2): 210-218.

[16] Liu X, Liu J, Cao P, et al. Efficient prediction of unsteady piston winds in subway tunnels based on machine learning[J]. Journal of Wind Engineering and Industrial Aerodynamics, 2025, 262: 106111.

[17] Yin H, Tang Z, Yang C. Predicting hourly electricity consumption of chillers in subway stations: a comparison of support vector machine and different artificial neural networks[J]. Journal of Building Engineering, 2023, 76: 107179.

[18] Nam K, Heo S, Li Q, et al. A proactive energy-efficient optimal ventilation system using artificial intelligent techniques under outdoor air quality conditions[J]. Applied Energy, 2020, 266: 114893.

[19] Heo S, Nam K, Loy-Benitez J, et al. A deep reinforcement learning-based autonomous ventilation control system for smart indoor air quality management in a subway station[J]. Energy and Buildings, 2019, 202: 109440.

[20] Leung P C M, Lee E W M. Estimation of electrical power consumption in subway station design by intelligent approach[J]. Applied Energy, 2013, 101: 634-643.

[21] Kavga A, Thomopoulos V, Pischinas E, et al. Design and simulation of a greenhouse in a computational environment (ANSYS/FLUENT) and an automatic control system in a LABVIEW environment[J]. Simulation Modelling Practice and Theory, 2023, 129: 102837.

[22] Liu M Z, Zhu C G, Cui T, et al. An alternative algorithm of tunnel piston effect by replacing three-dimensional model with two-dimensional model[J]. Building and Environment, 2018, 128: 55-67.

[23] Camelli F E, Byrne G, Löhner R. Modeling subway air flow using CFD[J]. Tunnelling and Underground Space Technology, 2014, 43: 20-31.

[24] Zhang X S, Kong Y L, Yang Y, et al. Using tree-based machine learning models to predict diverse compost maturity via one-hot encoding: Model deployment, experimental validation, and practical application[J]. Waste Management, 2025, 205: 114981.

[25] Wang R P, Lam S K, Wu M Q, et al. Destination intention estimation-based convolutional encoder-decoder for pedestrian trajectory multimodality forecast[J]. Measurement, 2025, 239: 115470.

[26] Xiao L Y, Song J J, Xie X, et al. Enhanced medical image segmentation using U-Net with residual connections and dual attention mechanism[J]. Engineering Applications of Artificial Intelligence, 2025, 153: 110794.

[27] Yunita A, Pratama M I, Almuzakki M Z, et al. Performance analysis of neural network architectures for time series forecasting: a comparative study of RNN, LSTM, GRU, and hybrid models[J]. MethodsX, 2025, 15: 103462.

(编辑　XXX)